Soft Matter

Cooperative size sorting of deformable particles in porous media

Journal:	*Soft Matter*
Manuscript ID	SM-ART-02-2019-000300.R1
Article Type:	Paper
Date Submitted by the Author:	21-Mar-2019
Complete List of Authors:	O'Connell, Margaret; Princeton University, Chemical and Biological Engineering Lu, Nancy; Princeton University, Chemical and Biological Engineering Browne, Christopher; Princeton University, Chemical and Biological Engineering Datta, Sujit; Princeton University, Chemical and Biological Engineering

Soft Matter

ARTICLE TYPE

Cite this: DOI: 10.1039/xxxxxxxxxx

Cooperative size sorting of deformable particles in porous media

Margaret G. O'Connell,[a*] Nancy B. Lu,[a*] Christopher A. Browne,[a*] and Sujit S. Datta[a]

Received Date
Accepted Date

DOI: 10.1039/xxxxxxxxxx

www.rsc.org/journalname

Diverse applications—ranging from enhanced oil recovery, filtration, and lab on a chip sorting—rely on the flow-induced transport of deformable particles in porous media. However, how fluid flow can force such particles to squeeze through pore constrictions of complex geometries is poorly understood. Here, we study the transport of model deformable particles in millifluidic porous media with constrictions of tunable aspect ratio. We find that multiple particles can unexpectedly squeeze through large-aspect ratio constrictions, even when isolated particles cannot. This phenomenon arises from pairwise flow-mediated interactions between the particles: when one particle is trapped at a constriction, the increased fluid flow around it enables a second to squeeze past due to locally increased hydrodynamic stresses. This cooperative mechanism causes the particles to ultimately sort themselves by size through the pore space. By revealing a new mode of deformable particle transport in porous media, our work helps to inform real-world applications and provides a straightforward way to sort particles based on size.

1 Introduction

Many real-world and laboratory settings involve the flow of deformable particles through complex porous media. For example, a promising approach for enhanced oil recovery relies on the injection of preformed particle gels (PPGs) into a porous subsurface reservoir.[1,2] As the particles squeeze through the pore space, they expand, eventually clogging regions of higher permeability and diverting flow to harder to access pores. A similar process arises in dead-end filtration, which seeks to prevent deformable solutes from squeezing through the pores of a filtration membrane and its filter cake.[3,4] Another example is lab on a chip sorting, in which interconnected networks of micro-/milli-fluidic constrictions are used to separate elastic capsules and cells by size and deformability.[5–9] In all of these cases, the process by which deformable particles squeeze through pore constrictions—or instead get stuck—critically impacts subsequent transport through the entire medium. Being able to predict and control this behavior is thus both fundamentally interesting and practically important.

Even describing the transport of a single deformable particle through a single, axisymmetric constriction is challenging. This process involves an intricate coupling between particle deformation and local hydrodynamic stresses—which depend on particle geometry, internal permeability, the constriction geometry, and fluid properties.[10–17] Moreover, most constrictions in natural porous media and in micro-/milli-fluidic channels are not perfectly circular, but rather have sharp edges and large aspect ratios.[18–28] As a result, a particle trapped at the entrance to a constriction does not completely block it, and fluid can continue to flow around the particle. For sufficiently large flow rates, the hydrodynamic stresses can force the particle to squeeze through the constriction; however, the conditions that control this behavior are difficult to generally predict due to the complex three-dimensional structure of the flow field.

An additional complexity arises when considering the transport of *multi*-particle suspensions; flow-mediated interactions between the different particles can potentially alter how they deform, move, and distribute themselves spatially. However, investigations of such multi-particle interactions and their macroscopic consequences are lacking, despite indications that cooperative interactions can have dramatic effects in other settings including causing droplet break-up and changing how cells migrate.[29,30] As a result, our ability to predict and control the flow of deformable particles through complex porous media is limited.

In this paper, we study the transport of multiple deformable particles through millifluidic porous media. The media have rectangular constrictions of tunable aspect ratio. We find that constriction aspect ratio plays a key role in regulating particle transport under flow-controlled conditions. For large aspect ratios, multiple particles can squeeze through the constrictions even when isolated particles cannot. Direct visualization of the individual particles sheds light on the underlying physics: trapping of one particle at the entrance to a constriction increases fluid flow around it, enabling a second particle to be advected by the flow and pushed through the constriction. This pairwise, flow-mediated process depends on the sizes of the different particles; specifically, smaller particles advance before larger particles. This

[a] *Department of Chemical and Biological Engineering, Princeton University, Princeton, New Jersey, 08544, United States; E-mail: ssdatta@princeton.edu*
* These authors contributed equally to this work.

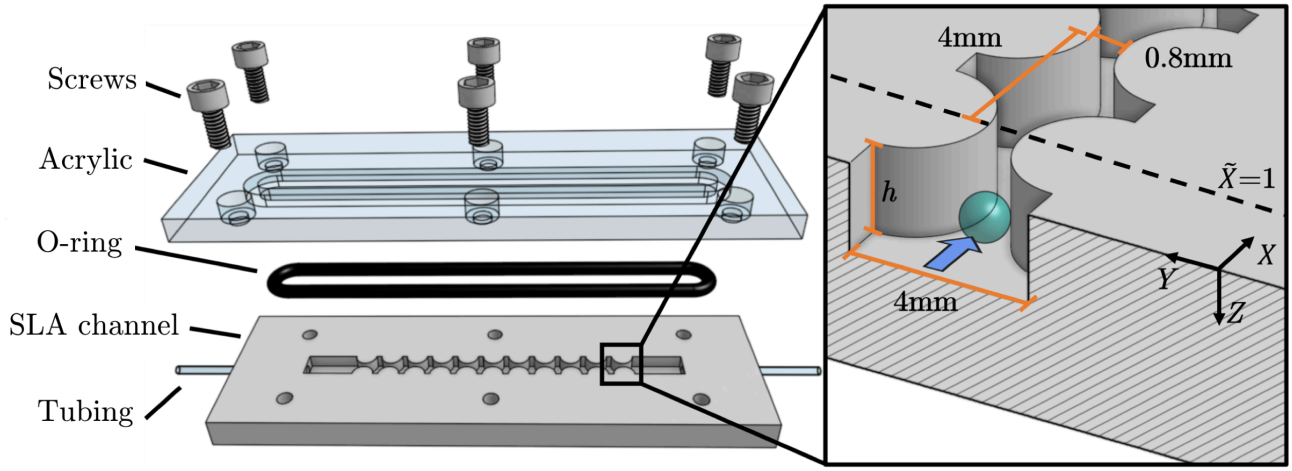

Fig. 1 Schematic of a millifluidic porous medium used to study deformable particle transport. Left panel shows assembly of the device; the flow proceeds in a 3D-printed stereolithography (SLA) channel that is sealed using an O-ring, a clear acrylic plate, and screws. Right shows dimensions of the flow channel and the pore constrictions. The channel height h is varied to obtain different constriction aspect ratios. Arrow indicates direction of imposed fluid flow. The position along the flow direction is denoted in dimensional form by X; the non-dimensional position is then given by $\tilde{X} \equiv 1+\Delta X/L$, where ΔX is the separation along the flow direction between the position of a particle center and the center of the first constriction, and $L = 4$ mm is the spacing between constrictions. The position of the first constriction thus corresponds to $\tilde{X} = 1$ as indicated by the dashed line.

size dependence causes the particles to autonomically and cooperatively sort themselves by size through the porous medium in a manner reminiscent of a *bubble sort* algorithm. Our results thus reveal new multi-particle effects in transport through a porous medium that may arise in applications; they also suggest a new way to sort polydisperse particles that could be applied in lab on a chip technologies.

2 Materials and Methods

The void space of a porous medium is typically composed of wide regions, known as pore bodies, connected by narrower—often rectangular—constrictions known as pore throats.[19,20,26–28] To represent these geometric features, we construct model porous media made of millifluidic channels with constrictions defined by evenly-spaced hemi-cylindrical posts as illustrated in Figure 1; a similar geometry has been used in previous investigations of flow through porous media.[31–33] Each channel is $W = 4$ mm wide, with opposing posts of diameter $D = 3.2$ mm that are laterally separated by 0.8 mm and spaced by $L = 4$ mm along the flow direction. The channel height, denoted by h, is either 0.8 mm or 2.4 mm; the constriction cross-section therefore has an aspect ratio $\alpha \equiv h/(0.8\text{ mm}) = 1$ or 3, respectively. The space between cylinders along the flow direction thus defines the pore bodies, while the lateral constriction between opposing cylinders defines the pore throats.

To fabricate the millifluidic devices, we use a novel 3D-printing approach that provides control over the channel geometry, and yields devices that can be optically interrogated while also withstanding high pressures. First, we 3D-print each open-faced channel with a FormLabs Form 2 stereolithography printer, using a proprietary clear polymeric resin (FLGPCL04) composed of methacrylate oligomers and photoinitiators. We then manually load test particles into a large well at the channel inlet. As model deformable particles, we use water-swollen polyacrylamide hydrogel beads (JRM Chemical) of diameter $D_p = 1.4 \pm 0.2$ mm and elastic modulus $E \approx 20$ kPa.[34] We then slowly fill each open-faced channel with the fluid phase at 0.1 mL/min, which exerts negligible hydrodynamic stresses on the particles. The fluid phase is deionized water with 1% green food coloring (McCormick & Co.); the coloring provides contrast and better visualization of the individual particles. Finally, we seal each channel with an overlying 1/8 inch thick clear acrylic plate, laser-cut to size. A water-tight seal is created using an O-ring fitted into a CNC-milled slot in the acrylic plate. Holes for screws are also drilled in the acrylic using the CNC mill, enabling each device to be screwed tight. The fully-assembled millifluidic device is mounted on an LED backlight panel; the acrylic is optically clear, enabling direct visualization of particle transport in the channels. Videos are captured by a mounted digital camera (Sony Alpha 6300) taking 4K resolution videos at 30 frames per second.

To enable fluid to flow, we insert 20-gauge needles into 1.4 mm diameter holes that horizontally connect to the inlet and outlet wells, and attach the needles to larger tubing. The needles are sufficiently small to prevent particle passage out of the millifluidic channel. We impose the flow through the tubing using a flow rate-controlled syringe pump (Harvard Apparatus PHD 2000). For the experiments reported here, the volumetric flow rate is fixed at $Q = 120$ mL/min to mimic flow-controlled conditions that often arise in oil recovery, filtration, and microfluidic applications.

3 Results

3.1 Influence of constriction aspect ratio

We first examine particle transport through media with constrictions of uniform aspect ratio ($\alpha = 1$). An isolated particle is initially advected by the flowing fluid, but becomes trapped at the constriction entrance, as shown in Figure 2A. This observation indicates that the particle cannot sufficiently deform due to the hydrodynamic stresses exerted by the fluid continuing to flow

around it. For this aspect ratio, we observe similar behavior with multiple particles as shown Figure 2B, indicating that interactions between particles do not play an appreciable role.

To quantify this behavior, we measure the particle positions as a function of time. The non-dimensional position is given by $\tilde{X} \equiv 1 + \Delta X/L$, where ΔX is the separation along the flow direction between the position of a particle center and the center of the first constriction, and L is the spacing between constrictions. The positions of the first, second, and third constrictions thus correspond to $\tilde{X} = 1$, 2, and 3, respectively. The non-dimensional time is given by $\tilde{T} \equiv TQ/V$, where T is the time elapsed after initializing the flow rate, $Q = 120$ mL/min is the volumetric flow rate, and the individual pore volume is given by $V = WLh - \pi D^2 h/4$. Consistent with the images shown in Figure 2A-B, particles cannot squeeze through the constrictions, as indicated by the flat profiles in Figure 2C.

We next examine the case of porous media with large-aspect ratio constrictions ($\alpha = 3$). An isolated particle again becomes trapped at the constriction entrance, similar to the case of $\alpha = 1$, as shown in Figure 2D and the red points in 2F. However, we observe dramatically different behavior when two particles are loaded into the inlet well. First, one particle is advected by the flowing fluid and becomes trapped at the constriction entrance (first panel in Figure 2E). The second particle is then advected toward the constriction, where it is rapidly pulled into the constriction by the increased fluid flow around the first particle (yellow points at $\tilde{T} \approx 50$ in Figure 2F). The hydrodynamic stresses cause the second particle to slowly deform and squeeze into the space above the first trapped particle (second panel in Figure 2E; $50 < \tilde{T} < 350$ in 2F), increasing the local fluid flow even further. The increased hydrodynamic stresses—which we estimate to be of order 10 kPa (Appendix A)—continue to deform both particles until the second is eventually able to pass through the constriction (third panel in Figure 2E; $\tilde{T} \approx 350$ in 2F). The second particle is then rapidly advected through the pore space at a speed ~ 10 cm/s, comparable to the interstitial flow speed Q/Wh, until it reaches the next constriction. The particle then remains trapped, similar to the case of an isolated particle (fourth panel in Figure 2E; $\tilde{T} > 400$ in 2F).

These observations indicate that particles can cooperatively transport through porous media with large-aspect ratio constrictions—even when isolated particles cannot. Specifically, the flow-mediated interactions between particles in a pair can enable one to squeeze into the space above another; the further increase in local flow causes one of the two particles to eventually squeeze through the entire constriction. While these interactions are challenging to quantify due to heterogeneous particle deformations and the complex three-dimensional flow field around a trapped particle, they can be described for specific geometries using numerical simulations.[10,13,15–17] We provide an estimate of the stresses arising during flow in Appendix A.

To further explore this cooperative transport process, we examine the case of three different particles in a medium with large-aspect ratio constrictions ($\alpha = 3$). A first particle initially becomes trapped at the first constriction entrance, as indicated by blue in the first panel of Figure 3A. A second particle is then pulled into the constriction by the increased fluid flow around the first particle (yellow in second panel of Figure 3A; $\tilde{T} \leq 250$ in 3B). This particle slowly deforms and squeezes through the constriction above the first particle (third panel of Figure 3A; $250 < \tilde{T} < 500$ in 3B), eventually passing through and reaching the next constriction, where it remains trapped (fourth panel of Figure 3A; $\tilde{T} > 500$). This pairwise process then repeats with a third particle (red in Figure 3): it is pulled into the first constriction, squeezes through, and eventually reaches the next constriction (fourth and fifth panels of Figure 3A; $500 < \tilde{T} < 750$). This third particle then squeezes through the space above the second particle and through the second constriction. The particle eventually reaches the third constriction (sixth panel of Figure 3A; $\tilde{T} > 750$), where it remains trapped as an isolated particle. The system reaches a steady state with each particle isolated in a separate pore; continued flow is unable to move them further. These observations indicate that multiple deformable particles can cooperatively transport themselves through porous media via sequential pairwise squeezing.

3.2 Size-sorting of particles

Close inspection reveals that when two particles are trapped at a large-aspect ratio constriction the increased local flow causes both to deform. This behavior is exemplified by the yellow and blue points between $50 < \tilde{T} < 350$ in Figure 2F; the positions of both particles increase gradually with time as they deform. We therefore expect that, for particles with similar mechanical properties and deformation rates, subsequent transit through the constriction will depend sensitively on the particle size—specifically, that the smaller of the two particles will pass through the constriction first. The results shown in Figure 2 support this expectation: the smaller of the two particles (yellow in Figure 2E-F) eventually squeezes through the constriction, while the larger particle (blue in 2E-F) instead relaxes back to its initial configuration.

The pairwise nature of this size sorting provides a strong analogy between deformable particle transport and computational sorting. Specifically, we propose that cooperative size sorting of deformable particles in a porous medium can be described as a *bubble sort* algorithm. This algorithm sorts a set of data by iteratively comparing each data element against its downstream neighbor, and swapping the pair if they are not in the right order. Consider, for example, a given string of characters: C A D B. In the description below, the red character is the element that is being pairwise compared and swapped downstream as needed:

Compare:	$\overrightarrow{\text{C A}}$ D B
Swap:	A C D B
Compare:	A $\overrightarrow{\text{C D}}$ B
Leave:	A C D B
Compare:	A C $\overrightarrow{\text{D B}}$
Swap:	A C B D
Compare:	$\overrightarrow{\text{A C}}$ B D
Leave:	A C B D
Compare:	A $\overrightarrow{\text{C B}}$ D
Swap:	A B C D
Compare:	A B $\overrightarrow{\text{C D}}$
Leave:	A B C D

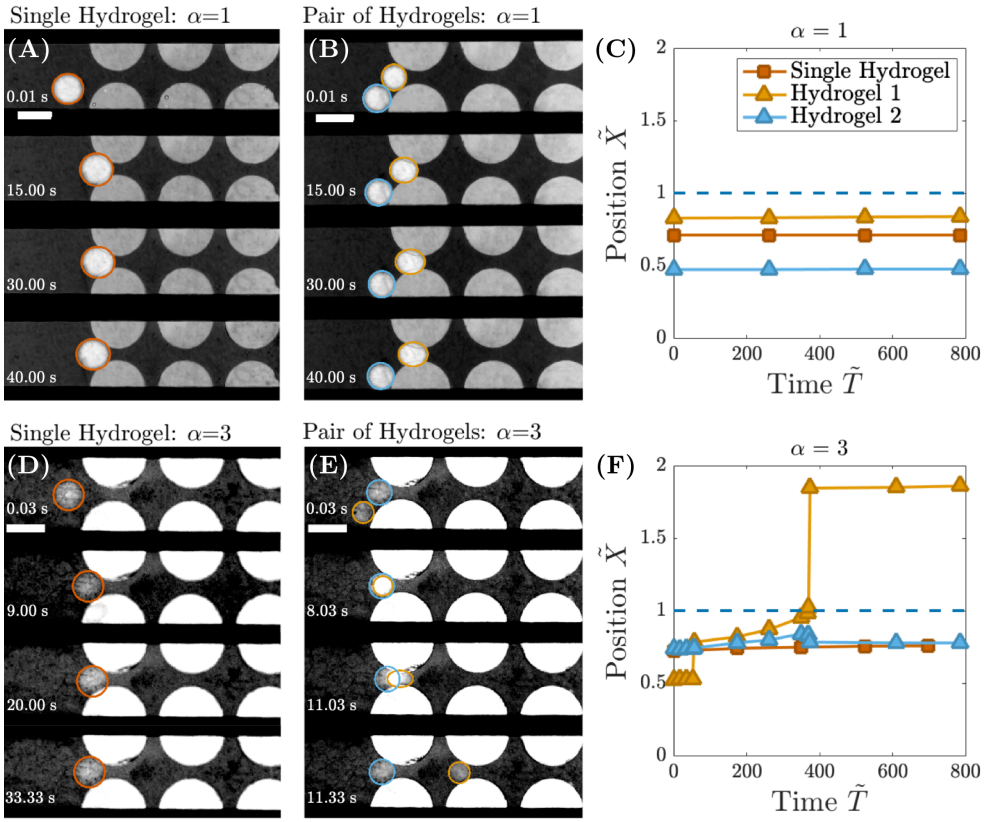

Fig. 2 Deformable particles squeeze in pairs through large-aspect ratio constrictions. Image snapshots (left) and plot (right) of hydrogel particle positions over time, for the case of a single or a pair of particles. Particles in a porous medium with constriction aspect ratio $\alpha = 1$ (A-C) are unable to squeeze through the constriction. Isolated particles in a channel with $\alpha = 3$ are also unable to squeeze through (D). By contrast, a particle can squeeze through the first constriction when paired with a second particle (E-F), but then remains trapped at the second constriction in isolation. Red points in C-F describe the single particle shown in panels A and D. Yellow and blue points in C and F describe the two different particles shown in panels B and E. Scale bars are 2 mm. Position and time in C and F are non-dimensionalized by the constriction separation and residence time of one pore volume of fluid, respectively, as described in the main text. The dashed line in C and F represents the center of the first constriction. Particles indicated by red, yellow, and blue points in (F) are 1.68 ± 0.03, 1.39 ± 0.04, and 1.55 ± 0.03 mm in diameter, respectively. Uncertainty is standard deviation in four distinct measurements of the diameter of each particle, representing the variability in particle size determination from imaging in the inlet chamber in the absence of flow. The difference in the particle sizes enables us to test the hypothesis that squeezing through a constriction is particle size dependent.

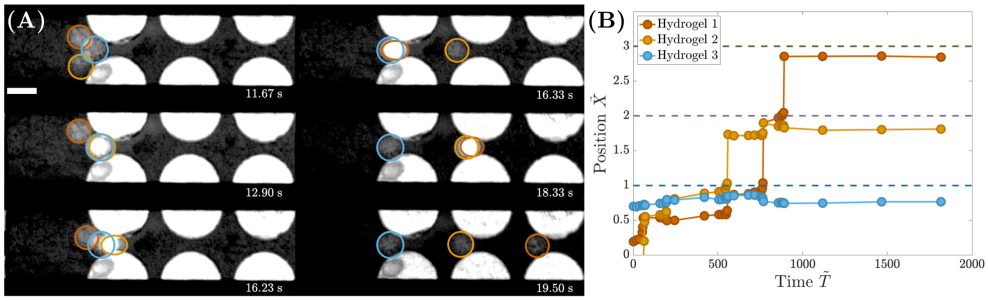

Fig. 3 Sequential pairwise squeezing of multiple particles in large-aspect ratio constrictions. Image snapshots (A) and plot (B) of hydrogel particle positions over time, for the case of three different particles in a porous medium with constriction aspect ratio $\alpha = 3$. One particle (blue) is initially trapped at the first constriction entrance, enabling a second particle (yellow) to squeeze through and reach the second constriction. Another particle (red) then squeezes through the first constriction and reaches the second as well. This particle then squeezes through the second constriction, enabled by a similar pairwise interaction, ultimately resulting in a steady-state distribution of particles through the medium. Scale bar is 2 mm. Position and time in B are non-dimensionalized by the constriction separation and residence time of one pore volume of fluid, respectively, as described in the main text. The dashed lines in B represent the centers of the first, second, and third constrictions ($\tilde{X} = 1, 2, 3$ respectively). Particles indicated by red, yellow, and blue points in (B) are 1.55 ± 0.02, 1.52 ± 0.02, and 1.56 ± 0.03 mm in diameter, respectively. Uncertainty is standard deviation in four distinct measurements of the diameter of each particle, representing the variability in particle size determination from imaging in the inlet chamber in the absence of flow.

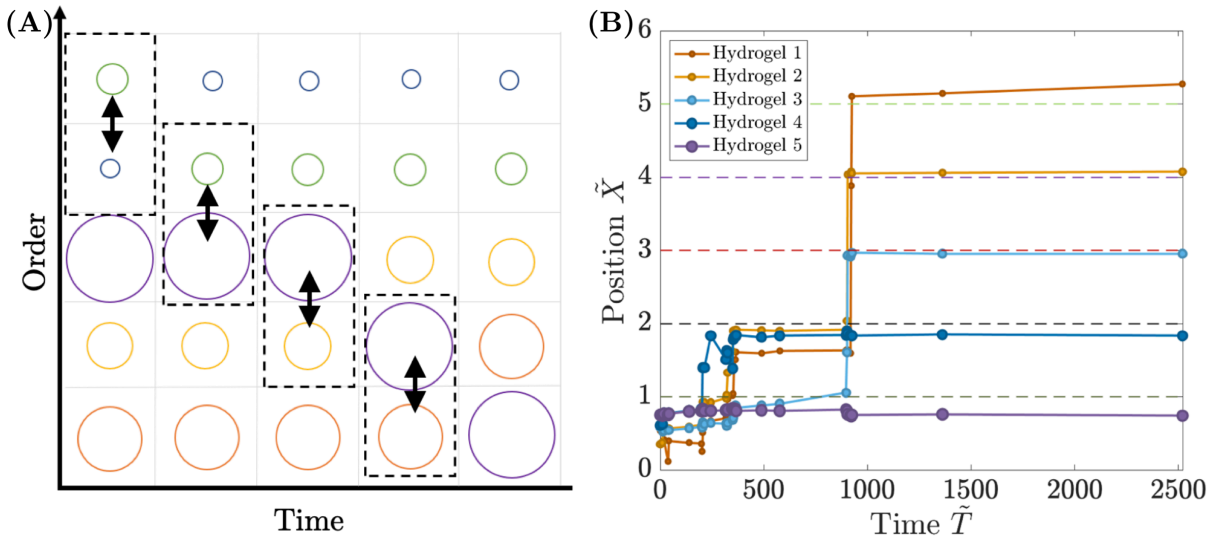

Fig. 4 Polydisperse particles exhibit sorting analogous to a bubble sort algorithm. (A) Schematic of bubble sort algorithm, showing how an initially unordered collection of polydisperse particles can order itself by size through successive, pairwise exchanges. (B) Experimental measurements of hydrogel particle positions over time, for the case of five different polydisperse particles in a porous medium with constriction aspect ratio $\alpha = 3$. The symbol sizes denote relative sizes of the particles. Through successive pairwise squeezing events, the particles sort themselves by size with the smaller particles being able to access the later pores. Position and time are non-dimensionalized by the constriction separation and residence time of one pore volume of fluid, respectively, as described in the main text. The dashed lines represent the centers of the first through fifth constrictions ($\tilde{X} = 1, 2, 3, 4, 5$ respectively). Particles indicated by red, yellow, light blue, dark blue, and purple points in (B) are 1.12 ± 0.01, 1.16 ± 0.01, 1.26 ± 0.01, 1.30 ± 0.01, and 1.53 ± 0.02 mm in diameter, respectively. Uncertainty is standard deviation in four distinct measurements of the diameter of each particle, representing the variability in particle size determination from imaging in the inlet chamber in the absence of flow.

The key feature of this process is the pairwise comparison of data elements, with individual elements being swapped downstream as needed—similar to the pairwise sorting of deformable particles through large-aspect ratio constrictions. To directly test this analogy, we investigate the transport of a polydisperse mixture of five hydrogel particles; the cooperative process by which we expect them to size-sort as they move through a porous medium with $\alpha = 3$ is schematized in Figure 4A. Even at this loading density, the particles pass through the medium one at a time due to pairwise interactions at each constriction similar to those described in Figures 2-3. In each particle pair, the smaller particle of the two squeezes through a constriction first and is advected through the pore space until it encounters a particle smaller than itself, analogous to the bubble sort algorithm, as shown in Figure 4B. Interestingly, this pairwise process appears to be independent of the order in which the particles reach the constriction—occurring even when the smaller particle reaches the constriction first. For example, particle 2 ($D_p = 1.16 \pm 0.01$ mm) reaches the second constriction well before particle 3 ($D_p = 1.26 \pm 0.01$ mm), which is larger; however, particle 2 does not squeeze through until particle 3 reaches the constriction as well, as shown by the yellow and light blue points at $\tilde{T} \approx 900$ in Figure 4B. As a result of this pairwise process, as flow progresses, all the particles in the channel successively squeeze through the porous medium until they are isolated at different constrictions. Subsequent fluid flow cannot further transport the particles, and their distribution remains at a steady state. Remarkably, at this steady state, the particles have sorted themselves from largest to smallest through the porous medium.

4 Conclusions

Our experiments reveal an unexpected mode of transport in which deformable particles cooperatively squeeze through large-aspect ratio constrictions in a porous medium, even when isolated particles cannot, under flow-controlled settings. Because constrictions with large aspect ratios arise in many natural and engineered porous media—including subsurface reservoirs, filters, and microfluidic devices—we expect that our findings will be broadly applicable.

This phenomenon relies on the increase in local flow when one particle is trapped at a constriction entrance, which pulls in another particle. The increased local hydrodynamic stresses deform and squeeze the particles into the constriction; the smaller of the pair can then pass through to the next constriction. The particle squeezing process is likely controlled by a complex coupling between the constriction geometry, particle geometry and elasticity, and the three-dimensional flow field around the trapped particles. Systematic investigation of the interplay between these factors, which likely determines the sensitivity of size-sorting, will be a valuable direction for future work.

Despite the complexity of the squeezing process, we show that this pairwise size-sorting can be modeled as a bubble sort algorithm, providing a general principle for modeling this process. As predicted by this algorithm, this cooperative process ultimately enables the particles to distribute themselves by size through the medium. This behavior must therefore be incorporated in transport models, which typically only consider particles in isolation and neglect inter-particle interactions. Importantly, this cooperative sorting is purely autonomic, requiring minimal external in-

tervention, suggesting a new way to sort deformable particles. We therefore anticipate that this mechanism could be applied in lab on a chip technologies that seek to sort droplets, cells, and particles by size.

5 Appendix A: Flow-induced stresses

Here, we estimate the characteristic stresses during particle trapping and squeezing. We first consider a particle of diameter $D_p \approx 1.4$ mm at the entrance to a constriction with uniform aspect ratio ($\alpha = 1$); due to the particle size, any other similar particles are obstructed from approaching the constriction. Our experimental observations (Figures 2A-B) indicate that the particle remains trapped, suggesting that the fluid continues to flow around the particle through small channels around it.[11,23] This observation suggests that the viscous pressure drop across the particle, ΔP_v, is less than the elastic stress required to squeeze the particle through the constriction, σ. Because the fluid channels formed around the particle are much smaller than the cross-section of the constriction, but much larger than the internal mesh of the particle itself (~ 6 nm for our experiments), we assume that the hydrodynamic resistance is dominated by flow through these channels. We then calculate the viscous pressure drop using Darcy's law, $\Delta P_v = \mu(Q\alpha/h^2)D_p/k$, where k is the fluid permeability through the channels around the particle. The squeezing process involves large particle deformations, and thus, accurately calculating the elastic stress requires consideration of non-linear elasticity. However, a simple estimate using linear elasticity yields $\sigma \approx E\varepsilon = 9$ kPa, where $\varepsilon \equiv 1-(h/\alpha)/D_p \approx 0.4$ represents the maximal strain during squeezing. The competition between the viscous pressure drop and the elastic stress required to squeeze the particle through the constriction is then given by the dimensionless ratio $C \equiv \Delta P_v/\sigma$. Our experiments indicate that the particle remains trapped, suggesting that $C < 1$, and thus, $k > 5\times10^{-10}$ m^2 in the case of a single particle with $\alpha = 1$.

For the case of a single particle with $\alpha = 3$, fluid primarily flows through the overlying open space $\approx (h-D_p)\times(h/\alpha)$ in area. An order-of-magnitude estimate of the corresponding maximal viscous pressure drop across the particle can be obtained assuming Hagen-Poiseuille flow through a cylindrical tube of length D_p and radius $\sqrt{(h-D_p)\times(h/\alpha)/\pi}$, $\Delta P_v \approx 8\pi\mu D_p Q/(h-D_p)^2(h/\alpha)^2 \approx$ 100 Pa; thus $C \sim 10^{-2} < 1$, and the particle remains trapped, as observed in the experiments. By contrast, when two particles are at the constriction entrance, we find that one is able to squeeze through (Figures 2E-F). This observation suggests that the viscous pressure drop across the particle, $\Delta P_v = \mu(Q\alpha/h^2)D_p/k$, is sufficient to balance the elastic stress required to squeeze the particle through the constriction, $\sigma \approx E\varepsilon = 9$ kPa—or in dimensionless form, $C \geq 1$. This criterion yields an estimate for the maximum fluid permeability through the channels around both particles: $k \leq 2\times10^{-10}$ m^2 for the case of a particle pair with $\alpha = 3$. Determining how this permeability threshold depends on the constriction geometry, particle geometry and elasticity, interactions between particles, and the three-dimensional flow field will be an important direction for future work.

Conflicts of interest

There are no conflicts to declare.

Acknowledgements

We would like to acknowledge Howard Stone for access to the FormLabs SLA printer. This work was supported by start-up funds from Princeton University, the Alfred Rheinstein Faculty Award, the Lidow Senior Thesis fund, and the ReMatch+ Summer Internship Program. This material is also based upon work supported by the National Science Foundation Graduate Research Fellowship Program (to C.A.B.) under Grant No. DGE-1656466. Any opinions, findings, and conclusions or recommendations expressed in this material are those of the authors and do not necessarily reflect the views of the National Science Foundation.

Notes and references

1 B. Bai, Y. Liu, J.-P. Coste and L. Li, *SPE Reservoir Evaluation & Engineering*, 2007, **10**, 176–184.
2 B. Bai, L. Li, Y. Liu, H. Liu, Z. Wang and C. You, *Preformed Particle Gel for Conformance Control: Factors Affecting Its Properties and Applications*, 04, 2007.
3 A. Gaveau, C. Coetsier, C. Roques, P. Bacchin, E. Dague and C. Causserand, *Journal of Membrane Science*, 2017, **523**, 446–455.
4 N. Lebleu, C. Roques, P. Aimar and C. Causserand, *Journal of Membrane Science*, 2009, **326**, 178–185.
5 P. Preira, V. Grandné, J. M. Forel, S. Gabriele, M. Camara and O. Theodoly, *Lab on a Chip*, 2013, **13**, 161–170.
6 L. K. Fiddes, E. W. Young, E. Kumacheva and A. R. Wheeler, *Lab on a Chip*, 2007, **7**, 863–867.
7 M. Chabert and J.-L. Viovy, *Proceedings of the National Academy of Sciences*, 2008, **105**, 3191–3196.
8 M. Abkarian, M. Faivre, R. Horton, K. Smistrup, C. A. Best-Popescu and H. A. Stone, *Biomedical Materials*, 2008, **3**, 034011.
9 L. Zhu, C. Rorai, M. Dhrubaditya and L. Brandt, *Soft Matter*, 2014, **10**, 7705–7711.
10 S. Kuriakose and P. Dimitrakopoulos, *Physical Review E - Statistical, Nonlinear, and Soft Matter Physics*, 2011, **84**, 011906.
11 C. N. Baroud, F. Gallaire and R. Dangla, *Lab on a Chip*, 2010, **10**, 2032–2045.
12 R. Kusters, T. Van Der Heijden, B. Kaoui, J. Harting and C. Storm, *Physical Review E - Statistical, Nonlinear, and Soft Matter Physics*, 2014, **90**, 033006.
13 S. Kuriakose and P. Dimitrakopoulos, *Soft Matter*, 2013, **9**, 4284–4296.
14 C. Rorai, A. Touchard, L. Zhu and L. Brandt, *European Physical Journal E*, 2015, **38**, 1–13.
15 Z. Y. Luo and B. F. Bai, *Soft Matter*, 2017, **13**, 8281–8292.
16 S. Y. Park and P. Dimitrakopoulos, *Soft Matter*, 2013, **9**, 8844–8855.
17 P. Dimitrakopoulos and S. Kuriakose, *Soft Matter*, 2015, **11**, 2782–2793.
18 D. R. Burns, C. H. Cheng and R. H. Wilkens, *International*

Journal of Rock Mechanics and Mining Sciences and, 1990, **27**, 315–323.
19 M. J. Kwiecien, I. F. Macdonald and F. A. Dullien, *Journal of Microscopy*, 1990, **159**, 343–359.
20 C. H. Cheng and M. N. Toksöz, *Journal of Geophysical Research: Solid Earth*, 1979, **84**, 7533–7543.
21 G. Tomaiuolo, M. Barra, V. Preziosi, A. Cassinese, B. Rotoli and S. Guido, *Lab on a Chip*, 2011, **11**, 449–454.
22 M. J. Fuerstman, A. Lai, M. E. Thurlow, S. S. Shevkoplyas, H. A. Stone and G. M. Whitesides, *Lab on a Chip*, 2007, **7**, 1479–1489.
23 S. A. Vanapalli, A. G. Banpurkar, D. Van Den Ende, M. H. Duits and F. Mugele, *Lab on a Chip*, 2009, **9**, 982–990.
24 B. J. Adzima and S. S. Velankar, *Journal of Micromechanics and Microengineering*, 2006, **16**, 1504–1510.
25 Y. Li, O. S. Sariyer, A. Ramachandra, S. Panyukov, M. Rubinstein and E. Kumacheva, *Scientific Reports*, 2015, **5**, 1–11.
26 Y. Bernabe, *Geophysics*, 1991, **56**, 424–576.
27 M. A. Ioannidis and I. Chatzis, *Chemical Engineering Science*, 1993, **48**, 951–972.
28 P. M. Doyen, *Journal of Geophysical Research*, 1988, **93**, 7729–7740.
29 L. Rosenfeld, L. Fan, Y. Chen, R. Swoboda and S. K. Tang, *Soft Matter*, 2014, **10**, 421–430.
30 J. O. Barber, J. M. Restrepo and T. W. Secomb, *Cardiovascular Engineering and Technology*, 2011, **2**, 349–360.
31 W. L. Olbricht, *Annual Review of Fluid Mechanics*, 1996, **28**, 187–213.
32 F. J. Galindo-Rosales, L. Campo-Deano, F. T. Pinho, E. van Bokhorst, P. J. Hamersma, M. S. N. Oliveira and M. A. Alves, *Microfluidics and Nanofluidics*, 2012, **12**, 485–498.
33 D. R. Graham and J. J. L. Higdon, *Journal of Fluid Mechanics*, 2002, **465**, 213–235.
34 N. Brodu, J. A. Dijksman and R. P. Behringer, *Nature Communications*, 2015, **6**, 1–6.